Reprinted from JOURNAL OF APPLIED METEOROLOGY, Vol. 35, No. 8, August 1996
American Meteorological Society

Aerosol Optical Properties in the Iranian Region Obtained by Ground-Based Solar Radiation Measurements in the Summer of 1991

TERUYUKI NAKAJIMA

Center for Climate System Research, University of Tokyo, Tokyo, Japan

TADAHIRO HAYASAKA, AKIKO HIGURASHI, AND GEN HASHIDA

Faculty of Science, Tohoku University, Sendai, Japan

NASER MOHARRAM-NEJAD, YAHYA NAJAFI, AND HAMZEH VALAVI

Department of the Environment of Iran, Tehran, Iran

(Manuscript received 16 August 1994, in final form 15 January 1995)

ABSTRACT

Solar radiation measurements were made using sun photometers and pyranometers during 31 May–7 June 1991 at several places in Iran and during 12 June–17 September 1991 at a fixed place, Bushehr, Iran. In the first period the aerosol optical thickness had values about 0.4 at the wavelength of 0.5 μm in the coastal area and about 0.2 in the plateau area. The Ångström's exponent, which is the slope of optical thickness spectrum, had values around 1 for large city areas and less than 0.5 for inland arid areas. Chemical analyses of sampled air indicate an effect of fossil fuel burning from local sources. Such optical and chemical characteristics of atmospheres suggest that soil-derived coarse particles contributed considerably to the atmospheric turbidity in arid areas, whereas an active generation of aerosols was dominant near large cities.

Significant rises in atmospheric turbidity were observed in the earlier part of the second period at Bushehr about once a week with a duration of about one day, which may have been caused by smoke from oil-well fires in Kuwait. The aerosol optical thickness in these events had values of about 1.5, which is equivalent to a columnar aerosol volume of 4.4×10^{-4} cm^3 cm^{-2}. The absorption index ranged from 0.005 to 0.02 with several peaks reaching 0.1 in the second period. These peaks can be attributed to prevailing smoke particles. In spite of the large variety of optical thicknesses and absorption indices, there existed stable power-law size distributions with an exponent about 3.7.

1. Introduction

There is recent recognition that anthropogenic aerosols cannot be ignored in global climate change issues. Recent GCM simulations have shown that an introduction of anthropogenic aerosol effects can improve the simulation of the global mean temperature records (Mitchell et al. 1995; Lacis and Mishchenko 1995). Through direct and indirect effects, the radiative forcing of anthropogenic aerosols may be comparable to the radiative forcing of greenhouse gases (Charlson et al. 1992). Such evaluation is, however, highly uncertain due to uncertainty in global-scale optical characteristics of aerosols. Aerosol absorption is, for example, one of highly uncertain parameters for the evaluation. The sign of the indirect effect can be changed by the magnitude of aerosol absorption (Kaufman and Nakajima 1993). There are, however, no good statistics of aerosol optical characteristics in Eurasian populated areas to study the aerosol climate effects. We should have more case studies of aerosol optical characteristics in these regions.

The Persian Gulf region has a heavy sand dust loading (Duce 1995) and anthropogenic sulphate emission (Langner et al. 1992), so that it is highly interesting to study the aerosol optical properties in this region. The aerosol characteristics in this region are expected to vary widely with complex aerosol sources such as heavy loading of atmospheric pollutant emitted by factories and automobiles in this area and dust loading by heavy dust storms. In particular, a large concentration of soil-derived aerosols is expected by large optical thicknesses in this region observed by NOAA AVHRR (Advanced Very High Resolution Radiometer) satellite images (Rao et al. 1988). However, there are few in situ measurements of dust properties, as compared with cases of dust storms in the Middle East and the Saharan

Corresponding author address: Dr. Teruyuki Nakajima, Center for Climate System Research, University of Tokyo, 4-6-1 Komaba, Meguro-ku, Tokyo 153, Japan.

regions (e.g., Joseph and Wolfson 1975; Carlson and Benjamin 1980; Fouquart et al. 1987; Tanre et al. 1988).

At the same time the oil-well fire events, caused by the Gulf War, made a large local climate effect around this region. The large-scale air pollution due to the Persian Gulf oil-well fires in 1991 caused by the Gulf War has been studied by many researchers (e.g., Browning et al. 1991; Bakan et al. 1991; Maryon and Buckland 1994; Husain 1994; Husain and Amin 1994) with concern about its serious effect on the local climate of the Persian Gulf region. For accurate assessment of the effect there have been extensive airborne measurements of the smoke plume, which spread along the Persian Gulf (Johnson et al. 1991; Weiss and Hobbs 1992). Relatively weak transport was found in the direction transverse to the smoke plume. The ratio of SO_2/CO_2 dramatically decreased with increasing distance due to rapid removal of SO_2. This observation leads to the conclusion that the oil-well fire smoke had small climatic effect except over a relatively limited area along the persistent smoke plume.

There have been few reports of air-quality observation, however, in areas other than relatively close to the smoke plume along the Saudi Arabian coast region. Therefore, it may be useful to make such measurements in the Iranian side of the Persian Gulf for improving our knowledge on the effect of smoke transport as well as the regional aerosol characteristics. For this purpose we have carried out solar radiation measurements and air sampling in the Iranian region and studied the effect of oil-well fire smoke as well as the microphysical characteristics of background aerosols in this region.

In this paper, we will report the result of our measurements and discuss the retrieved aerosol optical characteristics.

2. Instrumentation and measurements

We have performed solar radiation measurements and flask air sampling in the Iranian region in the period 31 May–17 September 1991 after the Gulf War, as a part of an oil-well fire study experiment organized by several universities in Japan and the department of the environment of Iran. Our measurements can be divided into two periods. The first period is 31 May–7 June 1991, when measurements were taken at several places along the route shown in Fig. 1 and Table 1. A sun photometer and pyranometer were set in an open place on the windward side of the road. We did not see noticeable evidence of the oil-well fire smoke effects at these observation sites, but we frequently encountered dust storms and some sites near large city areas suffered from heavy local air pollution. The second period is 12 June–17 September 1991, when similar measurements were made at a fixed site, the town of Bushehr, Iran (29.0°N, 50.8°E; 10 m MSL), almost every day at 1530, 1630, and 1730, Iranian standard time in this

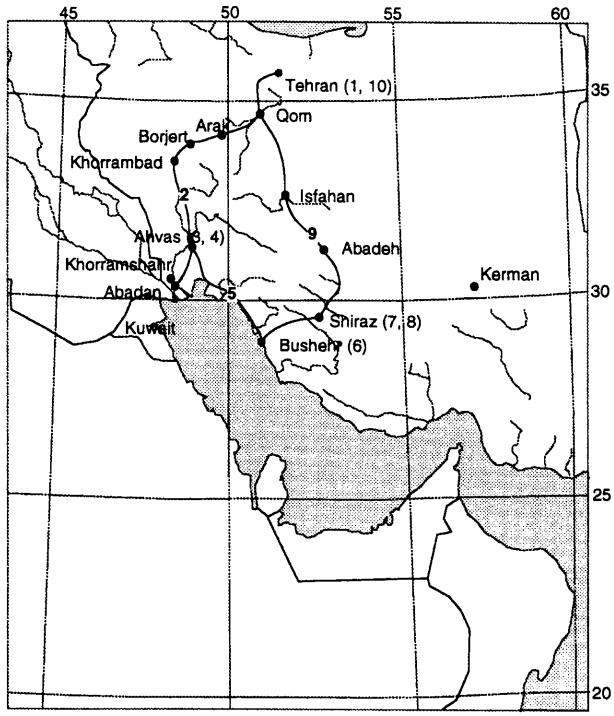

FIG. 1. Map of the measurement sites. The numbers on the map are the sample number cited in Table 2.

period (subtract 4.5 h to get the universal time). This site was frequently covered by heavy oil-well fire smoke almost every week, and it was reported that the local climate was cooler than average in the observation period. Local observers reported that the sun was obscured and the sky became very dark during the oil-well fire smoke events.

Two sets of four-channel portable sun photometers, EKO MS-120, were used for measuring spectral direct solar irradiance at wavelengths $\lambda = 0.368$, 0.500, 0.675, and 0.775 μm. The aerosol optical thickness $\tau_{a\lambda}$ has been calculated from the data as

$$\tau_{a\lambda} = \frac{\ln(F_{0\lambda}/F_{\lambda})}{m} - \tau_{m\lambda} - \tau_{0\lambda}, \qquad (1)$$

where $F_{0\lambda}$ is the direct solar irradiance that would be measured by the sun photometer at the top of atmosphere; $m = 1/\cos\theta_0$ is the solar optical airmass with the solar zenith angle θ_0; $\tau_{0\lambda}$ is the ozone optical thickness, and $\tau_{m\lambda}$ is the optical thickness of air molecules. We assumed a columnar ozone amount of 0.3 cm as a climatic average for calculating $\tau_{0\lambda}$ since the effect of ozone is small for estimating large aerosol optical thicknesses encountered in our analyses. The molecular optical thickness was obtained from Young (1981). The calibration constants $F_{0\lambda}$ of the two sun photometers were obtained by the Langley method. We also compared output readings of the two sun photometers

TABLE 1. Summary of sun photometer measurements during 31 May–7 June. Longitude ϕ, latitude λ, and height h of measurement sites and turbidity parameters $\tau_{0.5}$ and α are shown.

Date	λ (°N)	ϕ (°E)	h (m)	$\tau_{0.5}$	α	Comments
31 May	35.7°	51.4°	1500	0.14	1.59	Tehran, Azadi-Grand Hotel
1 June	35.7°	51.4°	1500	0.14	1.45	Tehran, Azadi-Grand Hotel
2 June	35.7°	51.4°	1500	0.38	1.25	Tehran, Azadi-Grand Hotel
2 June	34.5°	50.7°	1500	0.39	0.62	Before Arak, Desert with spotted grass, NW
2 June	33.9°	48.8°	1630	0.33	0.44	Borjerdo, SW2
3 June	31.3°	48.6°	50	0.25	0.62	Ahvas office roof, clear
3 June	30.8°	48.5°	30	0.16	0.40	Between Ahvas and Abadan, hazy
4 June	31.3°	48.6°	50	0.55	0.29	Ahvas office roof, Yellow dust, NNW5, large variation
4 June	31.2°	49.7°	130	0.55	0.40	Just after Ramhormoz
4 June	30.3°	49.6°	20	0.57	0.20	Before Hendijan
4 June	30.1°	50.1°	20	0.43	0.11	25 km to Vander-e-Deylam, W5
5 June	29.0°	50.8°	10	0.38	0.61	Bushehr hotel roof
6 June	29.0°	50.8°	0	0.21	0.88	Bushehr shore, clear
6 June	29.4°	51.4°	300	0.42	0.39	175 km to Shiraz, dust, yellow grass
6 June	29.6°	52.5°	1550	0.11	0.06	Shiraz environmental office roof
7 June	29.7°	52.8°	1580	0.29	1.24	Shiraz, NW1
7 June	30.6°	53.1°	2300	0.21	0.96	Deh Bid, dry bare land with spotted grass, clear
7 June	31.1°	52.7°	2000	0.12	0.87	10 km to Abadeh, bare land mixed with wheat field, NW4
7 June	33.4°	51.1°	2150	0.25	0.55	60 km to Delijan

at observation sites to reduce inconsistency in measurements made by the two sun photometers. Since the optical thickness reached as high as 2 on some occasions, we have corrected the effect of diffuse solar radiation by the method proposed in the appendix. According to the theoretical assessment this correction is equivalent to a correction of the optical thickness by less than about 0.1 even for slant optical paths $m\tau$ as large as 4.

Two pyranometers, EKO MS-801, were used for measuring the total downward solar radiative flux F (W m^{-2}). This pyranometer measures the downward radiative energy flux in solar wavelength region between 0.3 and 4 μm. We also measured the diffused solar radiative flux F_s by the solar occultation method making use of a shadowing disk to block the direct solar radiation. The effect of the finite size of the shadowing disk has been corrected in the same manner as in the sun photometer correction using theoretical radiative transfer calculations. Furthermore, in this case, we have integrated the corrected fraction over the wavelength range 0.3–4 μm.

We also sampled air in a glass flask for the first period at several places along the route. The sampling volume of the glass flask was 550 mL. The valve of the vacuum flask was opened windward to sample the air. The gas concentrations and carbon isotope ratio $\delta^{13}C$ were analyzed in the laboratory of Tohoku University. The concentrations of CO_2, CH_4, CO, and N_2O were analyzed by gas chromatographs (Shimazu Co. Ltd., GC-9A, and GC-14A) and the isotope ratio $\delta^{13}C$ was measured by a mass spectroscopy analyzer (Finnigan Co. Ltd., MAT-dE) of the National Institute of Polar Research.

3. Results

a. *Analyses of sun photometer data in the first period*

We summarize the results of sun photometer measurements in the first period (31 May–7 June) in Fig. 2 and Table 1. The data on each day are fitted by Ångström's law

$$\tau_{a\lambda} = \tau_{0.5}\left(\frac{\lambda}{0.5}\right)^{-\alpha}, \qquad (2)$$

where the λ's are wavelengths of the sun photometer channels. Averaged values of the turbidity factor $\tau_{0.5}$ and the Ångstöm exponent α at each site are also shown in the figure and table. We see values of about 0.4 near the coast and about 0.2 at the plateau of the inland area. The Ångström's exponent α widely varies over 0–1.6.

Taking the above results into account, we further study the aerosol properties of this region by the values of $\tau_{0.5}$ and α defined by Eq. (2). We find $\alpha \geq 1$ for large city areas such as Tehran and Shiraz, suggesting a large concentration of submicron particles and hence an active secondary aerosol generation. Most of other places, on the other hand, have small values as $\alpha \leq 0.5$. Especially, we have observed very small values of α around Ahvas, where we encountered turbid atmospheric condition with sand dust particles blown by strong wind. Nakajima et al. (1989) showed it is possible to explain a negative correlation between $\tau_{0.5}$ and α by growing aerosol particles with increasing relative humidity or by prevailing soil-derived particles. The characteristic value of α is about 1 for the former process and about 0 for the latter process. This difference comes from the difference in the characteristic size of

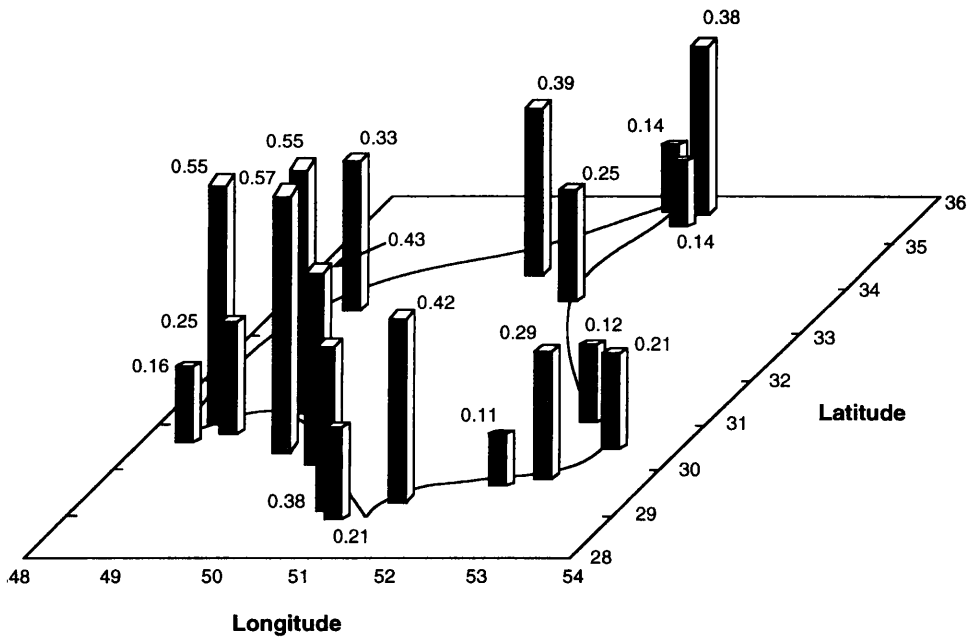

FIG. 2. Values of the turbidity factor in the period of 31 May–7 June 1991. Air sampling numbers in Table 2 are also shown in the figure.

aerosols associated with these processes. The former process is associated with submicron hygroscopic particles and the latter is with soil-derived dust particles of micron size. Values of α near 0 in Fig. 2 for large optical thicknesses suggest that dust particles rather than growing hygroscopic particles were responsible for much of the atmospheric turbidity. This is consistent with the fact that we observed intensive dust storms at several locations including Ahvas in the observation period.

Figure 3 shows the spectra of retrieved aerosol optical thicknesses $\tau_{a\lambda}$ for the cases shown in Fig. 2. Several patterns of wavelength dependence are found in this figure. The third dataset of 6 June (the Shiraz environmental office roof) has a small wavelength dependence with small optical thicknesses indicating prevailing soil-derived particles. On the contrary, data near large cities, such as Tehran datasets and the first dataset of 7 June taken at the city of Shiraz, have a large wavelength dependence with large optical thicknesses indicating prevailing small particles. These wide variations in the spectra suggest complex particle sources, for example, dust particles and accumulation mode aerosols generated by local pollution, which are also suggested by chemical gas analyses as shown below.

The origin of aerosols may be guessed from the chemical composition of sampled air. Air samples were taken at 10 points on the route from Tehran to Ahvaz, Busher, Shiraz, and back to Tehran. Table 2 shows the results of the analyses. We compared the results with data for the lower troposphere in Japan, which seem to be typical for northern midlatitudes, because we do not have the background data in Iran. Samples 1 and 10 taken in the Tehran city seem to be affected by contamination from local sources. In particular, such an effect is conspicuous for sample 10. The values for the other samples, however, have relatively small scatter in spite of the large area over which they were obtained. Accordingly, these values may be considered as typical for the air chemical composition in this region and in this season. Comparing these data with the corresponding values in Japan, some features are seen as follows: 1) the concentration of CO_2 is 10 ppmv higher than for Japan; 2) the concentration of CO is about three times higher than for Japan; 3) the value of $\delta^{13}C$ is 0.2‰ lower than for Japan. These features suggest the sampled air was strongly affected by fossil fuel combustion. It is very difficult to consider this feature as caused by the Kuwait oil-well fires, because the local and temporal variation of the chemical composition is very small. Consequently, we attribute this gaseous source to the many local oil factories and many automobiles without gas exhaust emission controls.

b. Analyses of sun photometer data in the second period

Solar radiation measurements at a fixed site in the town of Bushehr were carried out in the second period to observe the day-to-day variability of atmospheric turbidity. Figure 4 shows the time series of the turbidity parameters $\tau_{0.5}$ and α during this period (12 June–17 September 1991). The optical thickness had peaks as large as 1.5 occurring about once per week indicating

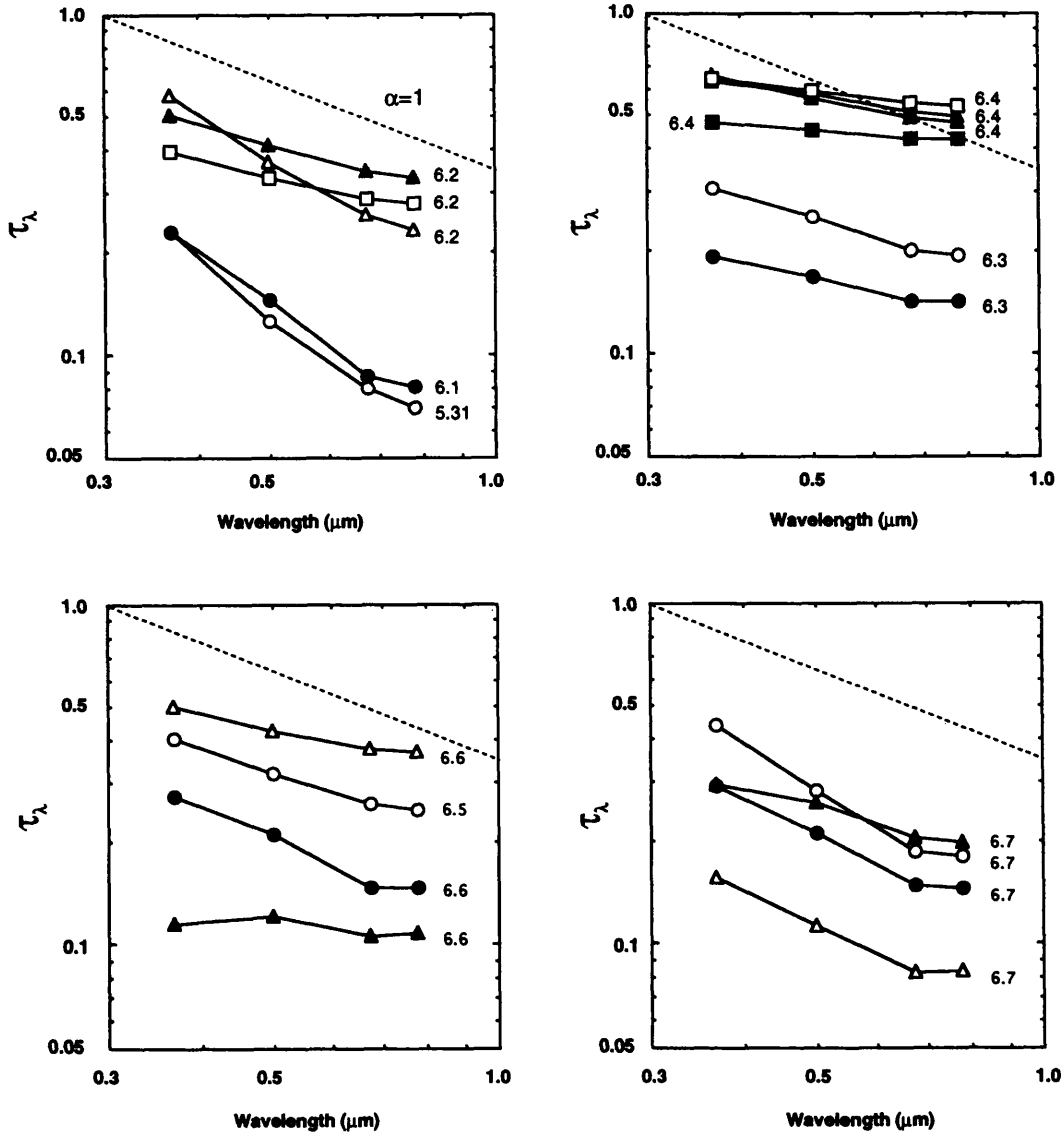

FIG. 3. Spectra of aerosol optical thickness in the period of 31 May–7 June 1991.

prevailing smoke from the oil-well fires of Kuwait. We have applied a correction to Eq. (1), as shown in the appendix, to derive the values of optical thickness, since the diffuse solar radiation contaminated the direct solar radiation signal for such large optical thicknesses. The correction needs the size distribution, for which we use a power-law size distribution determined by $\tau_{0.5}$ and α derived from Eq. (2) without correction,

$$\frac{dn}{dr} = \begin{cases} Cr^{-p}, & 0.1 < r \leq 10\ \mu\text{m} \\ \text{const}, & r \leq 0.1\ \mu\text{m} \end{cases}, \qquad (3)$$

with

$$p = 2.76 + 1.35\alpha. \qquad (4)$$

Equation (4) is slightly different from the well-known relationship $p = \alpha + 3$ taking into account the finite size range integration (Nakajima et al. 1983). Although we need an iteration to correct this initial size distribution, we did not iterate because the correction is at most 2.5% and iteration will not improve the result significantly.

The timescale associated with these peaks of the optical thickness is similar to the timescale of developing high and low pressure disturbances that were recorded by the local weather stations. This phenomenon may, therefore, be due to disturbing the narrow plume of the oil-well fire smoke blown by the seasonal northwest wind along the Persian Gulf. In fact the data at the meteorological office of Ahvas show a significant re-

TABLE 2. Chemical analyses of sampled air in the first period. The location of samples are depicted on the map of Fig. 1.

Samples	CO_2 (ppmv)	CH_4 (ppbv)	CO (ppbv)	N_2O (ppbv)	$\delta^{13}C$ (‰)
1	368.0	1796	560	314	−8.447
2	364.3	1776	440	312	−8.280
3	363.3	1788	500	315	−8.334
4	362.0	1790	490	313	−8.188
5	362.9	1793	460	316	−8.265
6	364.0	1802	510	309	−8.222
7	365.6	1803	530	311	−8.257
8	367.7	1838	510	320	−8.433
9	365.5	1754	440	315	−8.258
10	377.6	1939	2140	312	−8.997
Japan	356.0	1800	150	—	−8.040

duction of visibility occurred whenever a weak wind condition occurred. This suggests that the smoke diffused as a concentric puff from the source to surrounding areas in weak wind conditions. We will return to this point in trajectory analyses of the section for discussion. In the latter half of the period the time series of $\tau_{0.5}$ becomes smoother with fewer noticeable peaks. This may be explained by the fact that the seasonal wind system becomes more stable in the summer season. Decreases in smoke emission may not be the main reason, since the number of wells on fire and the particulate concentration measured along the coast of Saudi Arabia did not decrease significantly until late August (Husain and Amin 1994).

We show a scatterplot of $\tau_{0.5}$ versus α in Fig. 5 to study the correlation between the parameters for the results of Figs. 2 and 4. The Ångström exponent has a small variety at Bushehr with the typical value around 0.7, judging from values in the first and second periods (α at Bushehr in the first period are 0.61 and 0.88 as shown in Fig. 2). It should be noted that the town of Bushehr is located near the sea and is expected to have aerosol characteristics different from those of inland areas with small α. It is also interesting to find that points $\tau_{0.5} > 1$ corresponding to peaks of $\tau_{0.5}$ in Fig. 4 have similar Ångström's exponents around 0.7.

Figure 6 shows the wavelength dependence of spectral optical thicknesses of aerosols. It is found that $\log(\tau_{0.5})$ is nearly linear as a function of $\log(\lambda)$, indicating that Eq. (2) is a good approximation to the observed spectra. It is found, on the other hand, that the fitted values $\tau_{0.5}$ in the first period overestimate slightly the measured values $\tau_{a0.5}$, which means that the spectra tend to have a concave shape as a function of $\log(\lambda)$ as shown by Fig. 3. According to the inversion theory of the size distribution from optical thickness spectrum, bimodal or multimodal size distributions are responsible for such concave shape of the spectrum and consequently suggesting several aerosol sources. This observation is consistent with the discussion in section 3a.

c. *Analyses of solar radiative flux data*

King and Herman (1979) have shown that the absorption index, which is defined by the absolute value of the imaginary part of aerosol refractive index, and ground reflectivity can be estimated from the ratio of the spectral diffuse radiative flux to the spectral direct

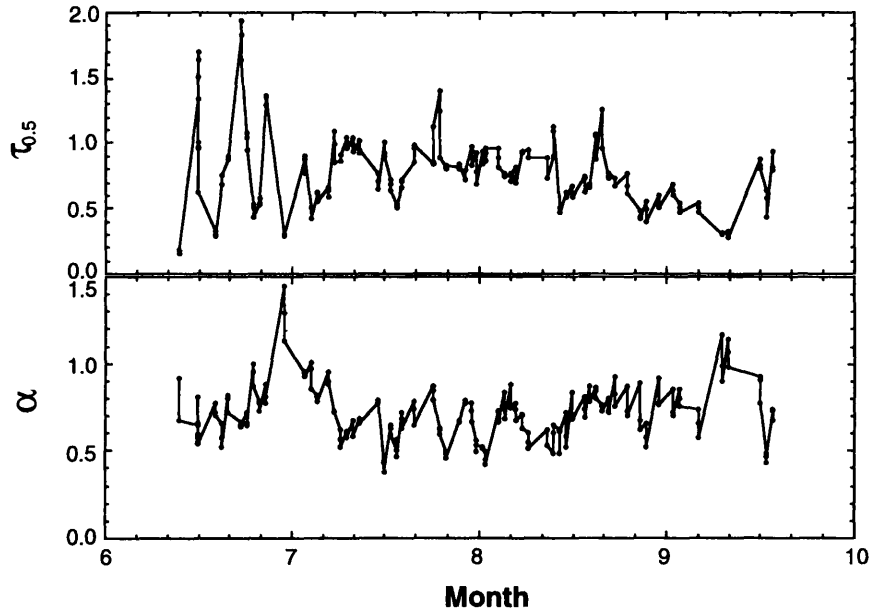

FIG. 4. Time series of the turbidity parameters at Bushehr in the period of 12 June–17 September 1991.

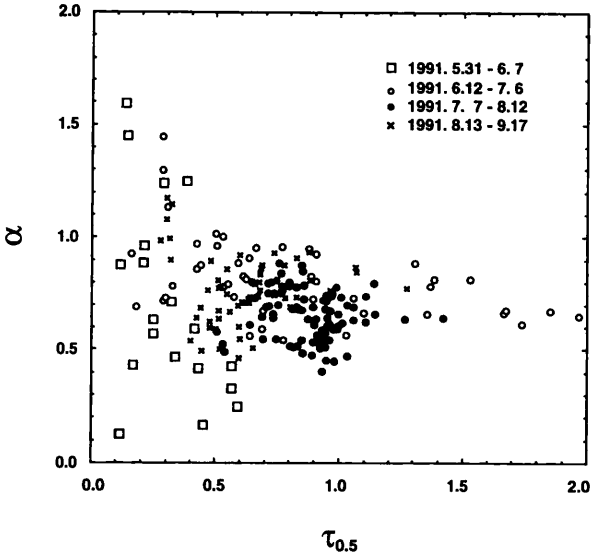

FIG. 5. Scatterplot of the turbidity factor versus exponent in the first and second periods.

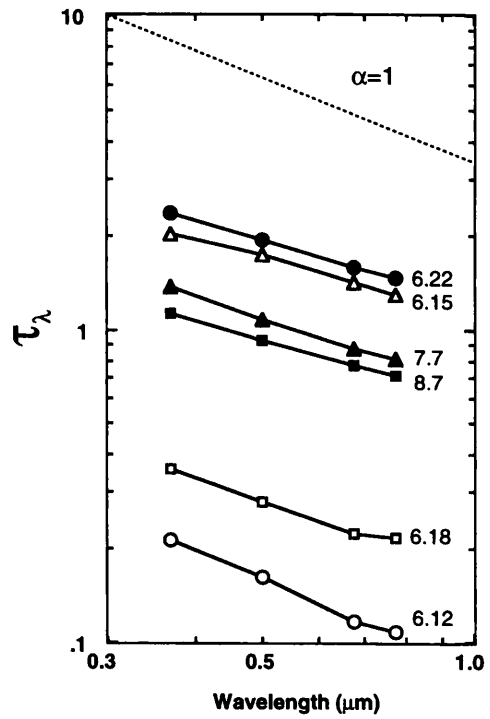

FIG. 6. Selected examples of aerosol optical thickness spectra at Bushehr in the period of 12 June–17 September 1991.

solar radiative flux. Similar information will be extracted analogously from direct and diffuse solar radiative fluxes integrated over wavelengths from 0.3 to 4 μm. The situation is illustrated in Fig. 7. We have simulated the direct and diffuse fluxes with column water vapor amount w = 1, 2, 4, and 8 g cm^{-2}; ground albedo A_g = 0, 0.1, 0.2, and 0.3; absorption index κ = 0, 0.01, 0.02, 0.03, and 0.05. Each line shows the dependence on one of these parameters when other parameters are fixed at reference values, that is, w = 2 g cm^{-2}, A_g = 0.1, and κ = 0.01. In the calculations we assumed θ_0 = 60° and $\tau_{0.5}$ = 0.5, which are typical values in the measurements at Bushehr as shown in Fig. 4, and with the power-law size distribution given in Eq. (3) with α = 1. Figure 7 shows that the diffuse flux mainly depends on absorption index and ground albedo, whereas the direct flux mainly depends on the water vapor amount. The sensitivity of diffuse flux to the absorption index is larger than to ground albedo.

From the above investigation we recognize that the following retrieval method is possible, extending the method of King and Herman for total solar radiative fluxes: 1) Get the size distribution from the measured aerosol optical thickness spectra by sun photometer and assuming Eqs. (3) and (4). 2) Calculate direct solar radiative fluxes with this size distribution and with several values of water vapor amount, which are compared with measured fluxes to determine water vapor amount. 3) Calculate diffuse solar fluxes with the derived optical thickness and water vapor amount for various values of κ. The absorption index is determined from comparison of theoretical and measured values of diffuse flux. Only one parameter that has to be assigned in this algorithm is the ground albedo at the measurement site.

The effect of ground albedo is, however, not so large as the effect of aerosol absorption index as shown in Fig. 7. We further investigate in Fig. 8 the sensitivities of the direct and diffuse fluxes to various parameters, such as the solar zenith angle θ_0, turbidity factor $\tau_{0.5}$, absorption index of aerosols κ, Ångström's exponent

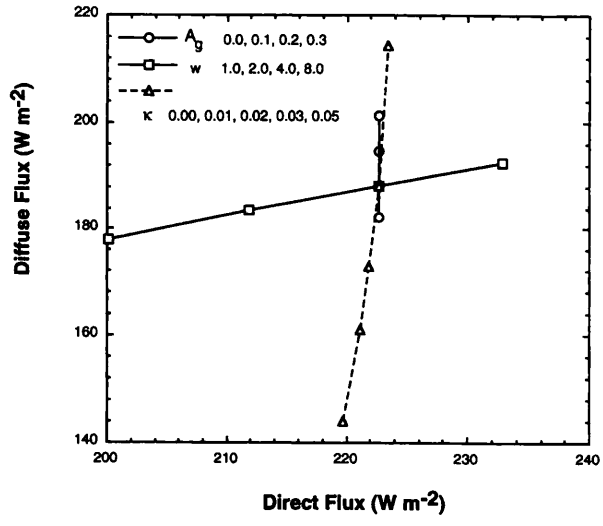

FIG. 7. Dependence of the direct and diffuse solar radiative fluxes on the ground albedo, columnar water vapor amount, and aerosol absorption index of refraction.

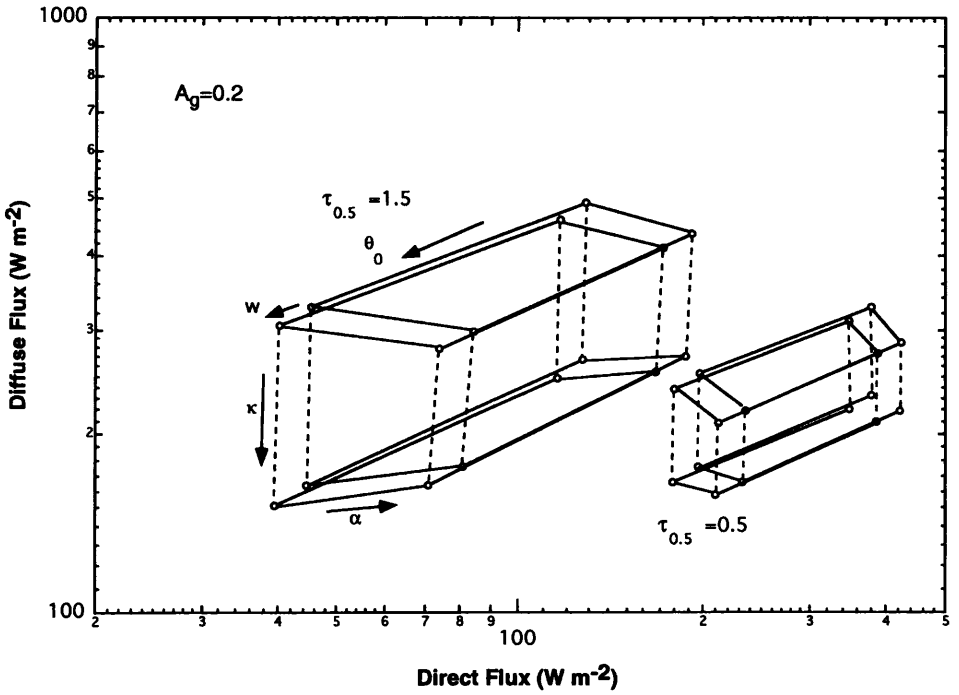

FIG. 8. As in Fig. 7 except for dependence on more parameters.

α, and water vapor amount w. From the figure it is seen that the dependence of κ on the direct and diffuse fluxes is different from that of other parameters, so that κ can be retrieved fairly well without serious problems. It is feasible, judging from Figs. 7 and 8, to get the water vapor amount and the aerosol absorption index from direct and diffuse solar radiative fluxes when we know the aerosol optical thickness from sun photometer data analyses.

Figures 9 and 10 show scatterplots of measured direct and diffuse fluxes for the first and second periods, respectively. To reduce the number of parameters to show, we corrected the effect of optical airmass and water vapor effects by using theoretical calculations. For this purpose the theoretical dependence of radiative

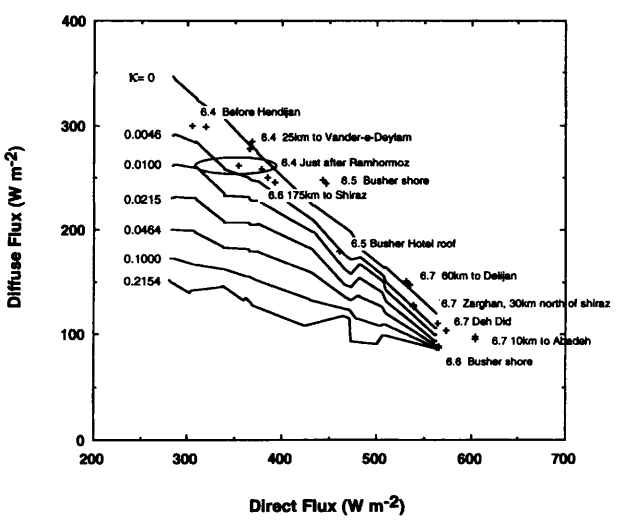

FIG. 9. Relationship between the diffuse and direct solar radiation fluxes in the period of 31 May–7 June 1991. Theoretical (solid lines with different values of κ) and observed (symbols) values are for the condition of m = 1.5 and w = 4 g cm^{-2}.

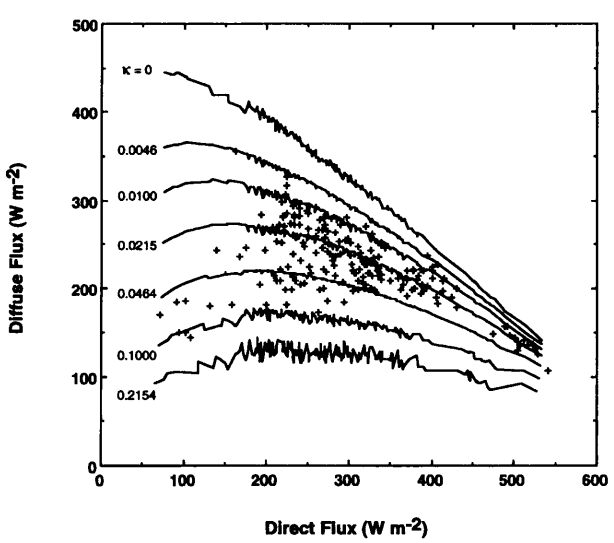

FIG. 10. As in Fig. 9 except for data at Bushehr in the period of 12 June–17 September 1991.

fluxes on optical airmass and water vapor amount have been calculated and applied to the measured values for obtaining the corresponding values at $m = 1.5$ and $w = 4$ g cm^{-2}. We used the power-law size distribution given by Eq. (3) with measured values of α in the calculations. Those corrected measured values are plotted by symbols in Figs. 9 and 10 together with the theoretical values. There are some fluctuations in the theoretical curves as revealed in the figures, since the theoretical values reflect the difference in aerosol size distributions.

It is found in Fig. 9 that aerosol absorption indices in the first period are smaller ($\kappa < 0.005$) than those in the second period. The unrealistic data points out of theoretical ranges might correspond to cases of broken clouds, which increase the diffused flux. Figure 10 shows, on the other hand, that the absorption index in the second period ranges between 0.01 and 0.03 for large direct flux, and the absorption index tends to increase when the direct solar radiation decreases. This means that the aerosol absorption index systematically decreases when the aerosol amount increases. This fact can be seen more clearly when we plot the retrieved values of the aerosol absorption index as in Fig. 11. Most of the retrieved values of the absorption index range from 0.01 to 0.03, but there are several cases with values as large as 0.1. Comparison with Fig. 4 shows that there is a correlation of large absorption index with peaks of the optical thickness. Hence, it is suggested that oil-well fire smoke particles have the absorption index as large as 0.1.

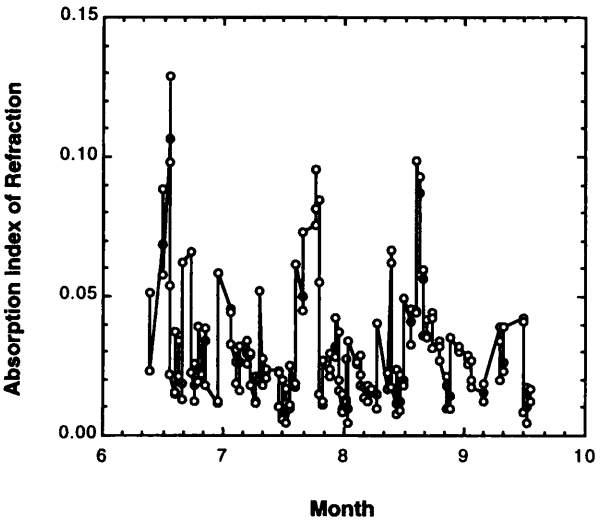

FIG. 11. Time series of retrieved absorption index of aerosols.

4. Discussion

To study the weather condition in the second period, we have made trajectory analyses using the ECMWF objective analysis dataset. Since the satellite imagery is an Eurlerian picture of the smoke flow at a fixed time, we have interpolated the three-dimensional position $P(t_{\text{AVHRR}}, t_{\text{start}})$ of airmass at the time of AVHRR images t_{AVHRR} with the parcel starting from the source at time t_{start}, among many trajectories along the wind vector (u, v, w) of the objective analysis data twice a day at 0000 and 1200 UTC and with pressure planes of 500, 700, 850, and 1000 hPa:

$$P(t_{\text{AVHRR}}, t_{\text{start}}) \leftarrow \{P(t_{\text{AVHRR}}, t_j - i\Delta) \mid i = 0, 1, \cdots; j = 1, \cdots, N\}, \quad (5)$$

where t_j is the consecutive time series of the wind velocity data and $\Delta = 1$ h is assumed. We calculated two trajectories assuming two point sources around Kuwait for each of the corresponding AVHRR images.

We have investigated 14 *NOAA-11* AVHRR images with the corresponding trajectories thus obtained. General matching of flow patterns is found as shown in Fig. 12 by three typical cases. Most of the trajectories are similar to that of 17 July with normal optical thickness at Bushehr. The case of 26 June corresponds to one of the peaks of optical thickness time series shown in Fig. 4 with $\tau_{0.5} = 1.37$, $\alpha = 0.79$, and $m_i = 0.034$. The trajectory shows the smoke was over Bushehr on this day. It is important to note that the smoke took more than one day for transportation. The case of 22 June corresponds to other peak of the optical thickness. Although the trajectory is not crossing Bushehr, the wind velocity was very small on this day as indicated by 1-h knots on the trajectory. For such conditions, our simple trajectory analyses may not be valid, and it is highly possible the smoke spread rather isotropically in this weak wind condition.

Taking into account the observation that local wind was generally weak when optical thickness rose, we made a comparison of the horizontal wind speed $u^2 + v^2$ at the sources, and a smoke index defined by $m_i\tau_{0.5}$ in Fig. 13. We have shifted the horizontal axis by 2 days for a horizontal wind speed plot allowing for transportation time. Figure 13 shows that there is a good correlation between the minima of horizontal wind speed and the maxima of the smoke index. From these observations, we can conclude that the atmosphere of Bushehr was largely contaminated by the smoke from oil-well fires on days of optical thickness rises as shown in Fig. 4.

If we closely investigate the time series of the turbidity factor in Fig. 4, it is found that the envelope of the minima in turbidity factors has a broad peak around the end of July. The following reasons can be considered to explain this phenomenon: 1) growing particles with increasing humidity, 2) an effect of the stratospheric aerosol layer formed by the eruption of the Pinatubo volcano, and 3) an increase of smoke particles. From the fact that the value of α decreases in this period reaching values as small as 0.4, it is suggested

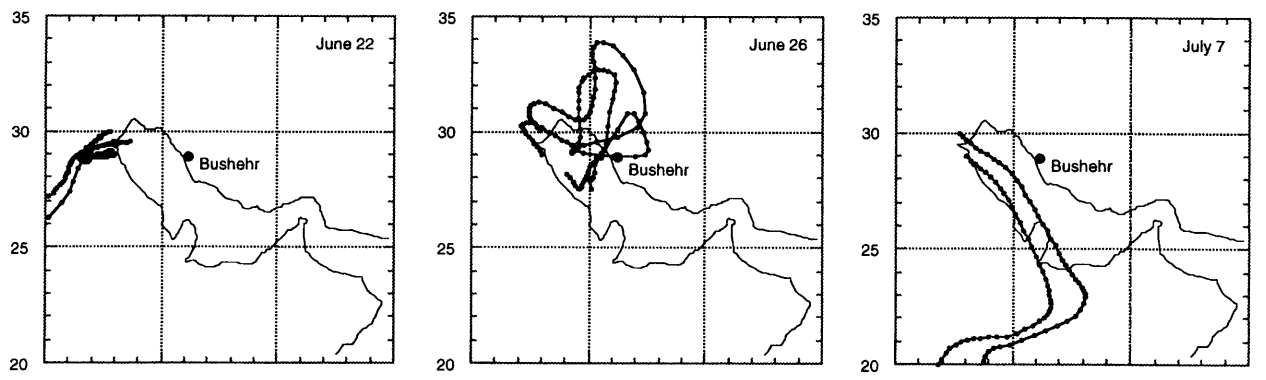

FIG. 12. Eurlerian trajectories of airflow for three characteristic cases. Two point sources are assumed. Knots on the trajectories show 1-h time interval.

that large particles were prevailing in this period. Enhanced stratospheric aerosols with mode radius around 0.6 μm such as for the El Chichon and Pinatubo aerosols are expected to have low values of $\alpha < 0.3$ (Nakajima et al. 1986; Asano et al. 1993). The globally averaged optical thickness of Pinatubo aerosols reached 0.29 in September (Minnis et al. 1993), although a large inhomogeneity was observed even in that period (Stowe et al. 1992). These facts suggest that Pinatubo aerosols are the most likely explanation for the reason of the broad hump in the optical thickness. On the other hand, it is difficult to explain this phenomenon by growing hygroscopic particles or smoke aerosols, since an increase of α will be expected with increasing these particles due to their large $\alpha \sim 0.7$. Furthermore there is no noticeable increase of κ around the broad peak, which should be caused by increasing smoke particles.

According to Figs. 4 and 5, the typical value of α is about 0.7 at Bushehr regardless of atmospheric condition. If we approximate the size distribution by a power-law function given in Eq. (3), we have $p = 3.7$, $Q_{ext} = 1.85$, and $\tau_{0.5}/V = 3.4 \times 10^4$ cm^2 cm^{-3}. This shows that the size distribution is near the Junge size distribution ($p = 4$) and Q_{ext} is about 2, which is the large particle limit. The maximum value about $\tau_{0.5} = 1.5$ is similar to values measured by Pilewskie and Valero (1992) in narrow intensive smoke plumes. This suggests that optical thicknesses of smoke layers did not change significantly even when smoke spread in weak wind conditions. If we assume $\tau_{0.5} = 1.5$ as the typical value of smoke optical thickness in the smoke events at Bushehr, we have the column aerosol volume $V = 4.4 \times 10^{-5}$ cm^3 cm^{-2}. The aerosol mass concentration is estimated to be $m_a = 590$ μg m^{-3} assuming 1500 m for the layer thickness (Weiss and Hobbs 1992; Husain 1994) and 2 g cm^{-3} for the aerosol density. This value is comparable with the measured values for the lower-soil-level cases of Cahill et al. (1992). In these lower-soil-level cases the contribution of soil-derived particles is less than 200 μg m^{-3}. They found there were high soil level cases with a much larger contribution of soil-derived particles ($\sim$1600 μg m^{-3}).

Weiss and Hobbs (1992) made in situ measurements of the aerosol single-scattering albedo. The retrieved values are about 0.58 almost independent of the distance from the oil-well fires. Figure 14 shows the scatterplot of $\tau_{0.5}$ and the aerosol single-scattering albedos at $\lambda = 0.75$ μm, which are calculated with derived absorption index in Fig. 11 and turbidity parameters in Fig. 4 together with the power-law size distribution in Eqs. (3) and (4). We have adopted the specific wavelength of 0.75 μm for the calculations, since the aerosol absorption indices obtained by the diffuse to direct ratio method is effective for the wavelengths from 0.75 to 1.0 μm, and the aerosol single-scattering albedo does not change significantly in this spectral range. It is found that the calculated single-scattering albedos ω_a have the following dependence on the absorption index κ:

$$\omega_a = 1 - \kappa^{(0.479 - 1.47\kappa + 5.41\kappa^2)}, \quad 0 \leq \kappa \leq 0.15.$$

The actual values scatter around this regression line depending on size distributions. The accuracy of the relationship is about 0.02. Figures 4, 11, and 14 show that smoke layers have an aerosol single-scattering albedo around 0.6–0.7. Weiss and Hobbs (1992) measured the single-scattering albedo around 0.52–0.60 in intense plume layers. This moderately large value of the single-scattering albedo is explained as a consequence of mixing of the black and white smoke plumes, which have large and small solar radiation absorptivities, respectively. The chemical and optical properties of black and white smoke plumes, taken from Weiss and Hobbs (1992) and Weiss et al. (1992), are summarized in Table 3. If we regard the smoke layer over Bushehr as a mixture of black and white smoke plumes, we have the following estimation of the mass soot particle fraction:

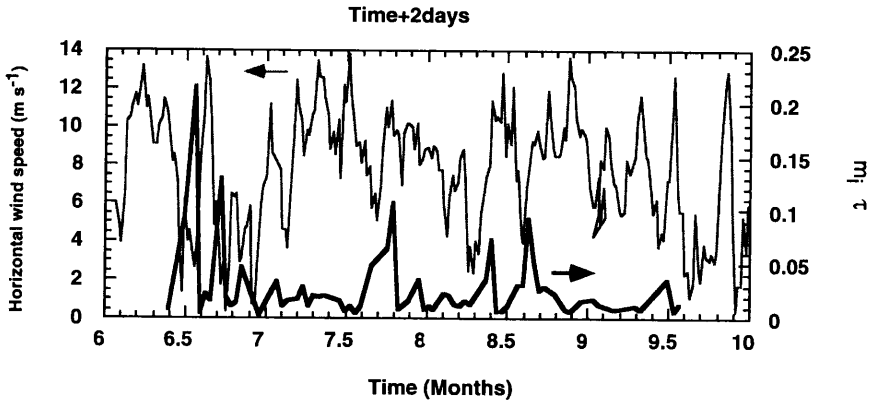

FIG. 13. Comparison of time series of horizontal wind speed (dotted line) and smoke index, $m_i\tau$ (solid line). The horizontal time axis is shifted by 2 days for horizontal wind speed plot.

$$\frac{M_{\text{soot}}}{M} = f_b B + f_w(1 - B) \tag{6}$$

$$1 - \omega_a = \frac{\sigma_b B + \sigma_w(1 - B)}{\sigma_b B(1 - \omega_b)^{-1} + \sigma_w(1 - B)(1 - \omega_w)^{-1}},$$

or

$$\frac{1}{B} = 1 + \frac{(\omega_a - \omega_b)\sigma_b/(1 - \omega_b)}{(\omega_w - \omega_a)\sigma_w/(1 - \omega_w)}, \tag{7}$$

where B is the mass fraction of black smoke, and σ_b and σ_w are the specific absorption coefficients for black and white smokes per unit mass. Using the values in Table 3, we have

$$B = \frac{3.15 - 3.5\omega_a}{2.95\omega_a - 0.7}. \tag{8}$$

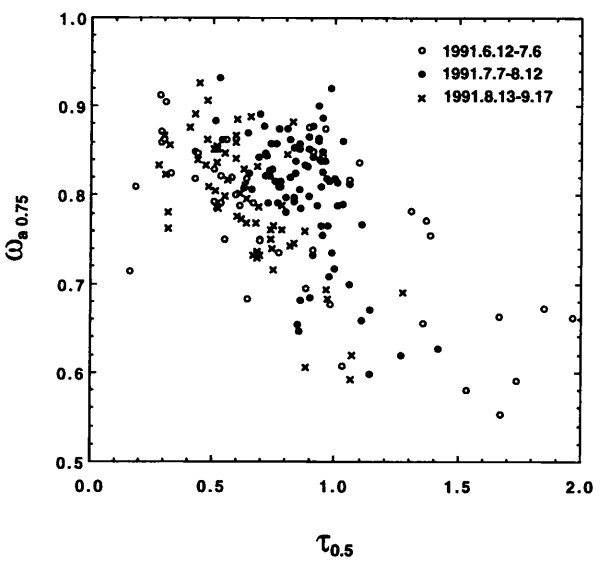

FIG. 14. Scatterplot of aerosol absorption index versus turbidity factor in the period of 12 June–17 September 1991.

For $\omega_a = 0.65$ as the mean value of the retrieved single-scattering albedo in the present study, we have $B = 0.33$ and $M_{\text{soot}}/M = 16\%$, whereas we have $B = 0.51$ and $M_{\text{soot}}/M = 22\%$ for $\omega_a = 0.56$, which is the mean value for intense smoke plumes measured by Weiss and Hobbs (1992). There is a slight reduction in the mass soot fraction during smoke transport to Bushehr area.

5. Summary

We have performed solar radiation measurements in Iran in two periods, 31 May–7 June and 12 June–17 September. In the first period, data were taken at several locations shown in Fig. 1. In the second period, data were taken almost every day at Bushehr as shown in Fig. 4. These are our findings:

1) In the first period, we observed $\tau_{0.5} \sim 0.4$ in the coastal area around Ahvas and $\tau_{0.5} \sim 0.2$ in the plateau area. There is a large scatter in the value of α. Small values of α suggests prevailing large soil-derived particles. High concentrations of CO_2 and CO and lower values of $\delta^{13}C$ suggest the effect of a combustion of fossil fuel and consequently an active generation of aerosols near large cities. Soot emission is small, however, without noticeable effect on the absorption index of aerosols.

2) In the earlier half of the second period, June, we observed significant increases in the atmospheric turbidity at Bushehr about once per week with about one day duration. This may be caused by a spreading puff of oil-well fire smoke around the source when the seasonal wind weakened. In these events the value of $\tau_{0.5}$ reached about 1.5, which corresponds to the aerosol column volume of about 4.4×10^{-5} cm^3 cm^{-2}. The peak in the atmospheric turbidity disappeared in the latter half of the observation period (July, August). This may be explained by the stabilizing seasonal wind system in the summer season. Power-law size distributions with $\alpha \sim 0.7$ were dominant at Bushehr in the whole period regardless of the oil-well fire events.

TABLE 3. Averaged chemical and optical properties of black and white smoke plumes.

Quantities	Symbol	Black smoke	White smoke	References
Mass soot fraction (%)	f	40	4	Weiss et al. (1992)
Specific absorption coefficients ($m^2\ g^{-1}$)	σ	4.0	0.35	Weiss and Hobbs (1992)
Single-scattering albedo	ω	0.38	0.90	Weiss and Hobbs (1992)

3) The envelope of minima of atmospheric turbidity in the second period had a broad hump at the end of July. The turbidity factor became as large as 0.8. An effect of Pinatubo aerosols is a likely explanation for this phenomenon.

4) Direct and diffuse solar radiative fluxes measured by pyranometer are found to be useful to get the column water vapor amount and the aerosol absorption index if the measured optical thickness is included in the analysis. Retrieved values of the absorption index range over 0–0.005 for the first period over a wide area of Iran; and over 0.01–0.03 for the second period at a fixed site, Busher. Values as high as 0.1 are found when the optical thickness reaches peak values in early July, showing that aerosols in these events had a large light absorption. The single-scattering albedo of aerosols is estimated to be 0.6–0.7, which corresponds to the mass soot fraction of about 16%.

Analyses of the measured data in the Iranian region have shown many interesting features, which are not found in the typical atmospheric environment in the middle latitudes, even without oil-well fire smoke events. This is partly because of the desert-type environment and partly because of heavy air pollution in the hot climate. It will be important to realize further measurements on long-term basis to understand these features we have observed.

Acknowledgments. One of us is grateful to Prof. T. Matsuno of Hokkaido University, and Drs. Michael D. King and Thomas L. Bell of NASA Goddard Space Flight Center for their valuable advice and support. We are also grateful to the experiment team members lead by Prof. Y. Iwasaka of Nagoya University for supporting measurements. We received good advice from Dr. M. Shiobara of the Japanese Meteorological Institute on correcting the sun photometer data. The sun photometers used in this study were provided by EKO Instrument Company and Asia Aviation Company. We are thankful to them for their kind support.

APPENDIX

Correction to Sun Photometery and Pyranometry

For large optical thicknesses, the retrieval of optical thickness from the sun photometer is difficult since there is a contamination of diffused solar radiation (Shiobara and Asano 1994)

$$F_{\text{obs}} = F_{\text{true}} + E_s, \tag{A1}$$

where F_{obs} is the observed direct solar irradiance and F_{true} is the true direct solar irradiance as defined

$$F_{\text{true}} = F_0 \exp(-m\tau), \tag{A2}$$

$$m = \frac{1}{\cos\theta_0}. \tag{A3}$$

The observed solar irradiance is the sum of the true irradiance plus the sky radiation contribution E_s integrated over the field of view of the sun photometer $\Delta\Theta$ as

$$E_s = 2\pi \int_0^{\Delta\Theta} L(\Theta, \Phi) \cos\Theta \sin\Theta d\Theta. \tag{A4}$$

According to Box and Deepak (1981), the circumsolar sky radiance can be approximated by their MS method

$$L = mF_{\text{true}}[(\omega_m\tau_m + \tau_{ms})P_m + \tau_{as}P_a + \tau_g P_m(0)], \tag{A5}$$

where

$$\tau_{ms} = 0.02\tau_{ss} + 1.2\tau_{ss}^2 m^{1/4}, \tag{A6}$$

$$\tau_{ss} = \omega_a\tau_a + \omega_m\tau_m, \tag{A7}$$

$$\tau_{as} = \omega_a\tau_a, \tag{A8}$$

$$\tau_g = \frac{A_g\tau_2}{1 - A_g\tau_3}, \tag{A9}$$

$$\tau_2 = 1.34\frac{\tau_{ss}}{m}[1 + 0.22(m\tau_{ss})^2], \tag{A10}$$

and

$$\tau_3 = 0.9\tau_{ss} - 0.92\tau_{ss}^2 + 0.54\tau_{ss}^3. \tag{A11}$$

In Eqs. (A5)–(A9), ω_m and ω_a are the single-scattering albedos of molecules and aerosols; A_g is the ground albedo; P_m and P_a are the phase functions of molecules and aerosols, respectively. From Eqs. (A1)–(A11), we get the following expression for an index to indicate the deviation between F_{obs} and F_{true},

$$\rho \equiv \frac{F_{\text{obs}} - F_{\text{true}}}{mF_{\text{true}}} = \frac{E_s}{mF_{\text{true}}}$$

$$= 2\pi \int_0^{\Delta\Theta} [(\omega_m\tau_m + \tau_{ms})P_m + \tau_{as}P_a + \tau_g P_m(0)] \times \cos\Theta d\cos\Theta$$

$$\approx 2\pi \int_0^{\Delta\Theta} [(\omega_m\tau_m + \tau_{ms})P_m(0) + \tau_{as}P_a + \tau_g P_m(0)] d\cos\Theta. \tag{A12}$$

If we defined the following average,

$$\langle f \rangle \equiv 2\pi \int_0^{\Delta\Theta} f(\cos\Theta) d\cos\Theta,$$

we can write the solid view angle of the sun photometer and ρ as follows:

$$\Delta\Omega \equiv \langle 1 \rangle = \pi(\Delta\Theta)^2, \quad \text{(A13)}$$

$$\rho \approx (\omega_m\tau_m + \tau_{ms} + \tau_g)P_m(0)\Delta\Omega + \tau_{as}\langle P_a \rangle, \quad \text{(A14)}$$

where

$$\langle P_a \rangle \equiv 2\pi \int_0^{\Delta\Theta} P_a(\cos\Theta) d\cos\Theta = \bar{P}_a\Delta\Omega. \quad \text{(A15)}$$

Finally, we have

$$\rho \approx \left[(\omega_m\tau_m + \tau_{ms} + \tau_g)\frac{3}{8\pi} + \tau_{as}\bar{P}_a \right]\Delta\Omega. \quad \text{(A16)}$$

To use Eq. (A16), we have to know the averaged aerosol phase function value, ground albedo, and single-scattering albedos of molecules and aerosols in addition to the observed aerosol optical thickness. Parameters other than the averaged aerosol phase function do not affect the results much, so that we can assume $A_g = 0$, $\omega_m = 1$, and $\omega_a = 1$ for most applications. The averaged aerosol phase function strongly depends on the aerosol size distribution. In the case of a power-law size distribution, we have the following approximation in terms of λ and α,

$$\bar{P}_a = Ce^{-\gamma\alpha}, \quad \text{(A17)}$$

$$C = 19.1 - 101\ln(\lambda), \quad \text{(A18)}$$

$$\gamma = 3.34 - 1.18\lambda. \quad \text{(A19)}$$

The averaged phase function value is also dependent on $\Delta\Theta$. In the above expression we have assumed $\Delta\Theta = 1.65°$, which is the half view angle of EKO MS-120.

Figure A1 shows the ρ value calculated numerically by a full radiative transfer scheme as a function of $m\tau$ (Nakajima and Tanaka 1986). As expected from the approximation, the ρ value does not depend strongly on the solar zenith angle, so that values with $\theta_0 = 60°$ are shown in the figure. The effect of the diffuse radiation reaches 10% of the true direct irradiance when $m\tau = 4$ and $p = 3.5$, whereas it is less than 4% if $p = 4.0$. This means the error involved in the retrieved optical thickness without correction will be 2.5% at maximum. This is small enough that we decided to correct the received irradiance as follows: 1) get the optical thickness without correction; 2) find the effect of diffuse radiation with this optical thickness; 3) find the improved optical thickness with correction of diffuse radiation.

We integrate the above expression in the solar spectral region for estimating the effect of the finite shadowing disk used in diffuse flux measurements and correct this effect in the same manner as in the sun photometer correction.

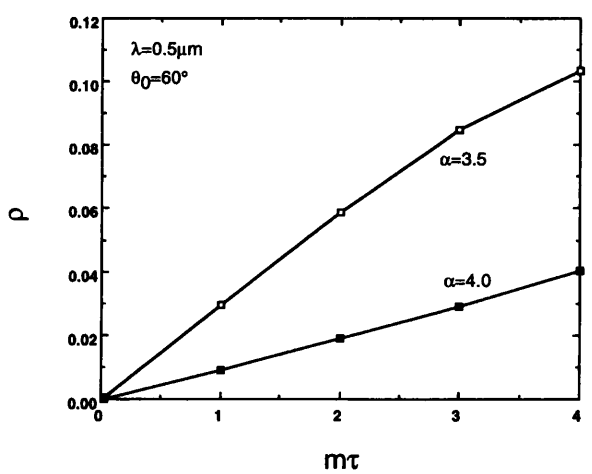

FIG. A1. The ρ value as a function of $m\tau$.

REFERENCES

Asano, S., A. Uchiyama, and M. Shiobara, 1993: Spectral optical thickness and size distribution of the Pinatubo volcanic aerosols as estimated by ground-based sunphotometry. *J. Meteor. Soc. Japan,* **71,** 165–173.

Bakan, S., and Coauthors, 1991: Climate response to smoke from the burning oil wells in Kuwait. *Nature,* **351,** 367–371.

Box, M. A., and A. Deepak, 1981: An approximation to multiple scattering in the earth's atmosphere: Almucantar radiance formulation. *J. Atmos. Sci.,* **38,** 1037–1048.

Browning, K. A., and Coauthors, 1991: Environmental effects from burning oil wells in Kuwait. *Nature,* **351,** 363–367.

Cahill, T. A., K. Wilkinson, and R. Schnell, 1992: Composition analyses of size-resolved aerosol samples taken from aircraft downwind of Kuwait, spring 1991. *J. Geophys. Res.,* **97,** 14 513–14 520.

Carlson, T. N., and S. G. Benjamin, 1980: Radiative heating rates for Saharan dust. *J. Atmos. Sci.,* **37,** 193–213.

Charlson, R. J., S. E. Schwartz, J. M. Hales, R. D. Cess, J. A. Coakley Jr., J. E. Hansen, and D. J. Hofmann, 1992: Climate forcing by anthropogenic aerosols. *Science,* **255,** 423–430.

Duce, R. A., 1995: Sources, distributions, and fluxes of mineral aerosols and their relationship to climate. *Aerosol Forcing of Climate,* R. J. Charlson and J. Heintzenberg, Eds., John Wiley & Sons, 43–72.

Fouquart, Y., B. Bonnel, M. C. Roquai, and R. Santer, 1987: Observations of Saharan aerosols: Results of ECLATS field experiment. Part I: Optical thickness and aerosol size distributions. *J. Climate Appl. Meteor.,* **26,** 28–37.

Husain, T., 1994: Kuwait oil fires—Modeling revisited. *Atmos. Environ.,* **28,** 2211–2226.

——, and M. B. Amin, 1994: Kuwait oil fires—Particulate monitoring. *Atmos. Environ.,* **28,** 2149–2158.

Johnson, D. W., C. G. Kilsby, D. S. McKenna, R. W. Saunders, G. J. Jenkins, F. B. Smith, and J. S. Foot, 1991: Airborne observations of the physical and chemical characteristics of the Kuwait oil smoke plume. *Nature,* **353,** 617–621.

Joseph, J. H., and N. Wolfson, 1975: The ratio of absorption to backscatter of solar radiation by aerosols during Khamsin conditions and effects on the radiation balance. *J. Appl. Meteor.*, **14,** 1389–1396.

Kaufman, Y. J., and T. Nakajima, 1993: Effect of Amazon smoke on cloud microphysics and albedo—Analysis from satellite imagery. *J. Appl. Meteor.*, **32,** 729–744.

King, M. D., and B. M. Herman, 1979: Determination of the ground albedo and the index of absorption of atmospheric particulates by remote sensing. Part I: Theory. *J. Atmos. Sci.*, **36,** 163–173.

Lacis, A. A., and M. I. Mishchenko, 1995: Climate forcing, climate sensitivity, and climate response: A radiative modelling perspective on atmospheric aerosols. *Aerosol Forcing of Climate,* R. J. Charlson and J. Heintzenberg, Eds., John Wiley & Sons, 11–42.

Langner, J., H. Rodhe, P. J. Crutzen, and P. Zimmermann, 1992: Anthropogenic influence on the distribution of tropospheric sulphate aerosol. *Nature,* **359,** 712–716.

Maryon, R. H., and A. T. Buckland, 1994: Diffusion in a Laglangian multiple particle model: A sensitivity study. *Atmos. Environ.*, **28,** 2019–2038.

Minnis, P., E. F. Harrison, L. L. Stowe, G. G. Gibson, F. M. Denn, D. R. Doelling, and W. L. Smith Jr., 1993: Radiative climate forcing by the Mount Pinatubo eruption. *Science,* **259,** 1411–1415.

Mitchell, J. F. B., T. C. Johns, J. M. Gregory, and S. F. B. Tett, 1995: Climate response to increasing levels of greenhouse gases and sulphate aerosols. *Nature,* **376,** 501–504.

Nakajima, T., and M. Tanaka, 1986: Matrix formulations for the transfer of solar radiation in a plane-parallel scattering atmosphere. *J. Quant. Spectrosc. Radiat. Transfer,* **35,** 13–21.

——, ——, and T. Yamauchi, 1983: Retrieval of the optical properties of aerosols from aureole and extinction data. *Appl. Opt.*, **22,** 2951–2959.

——, ——, T. Hayasaka, Y. Miyake, Y. Nakanishi, and K. Sasamoto, 1986: Airborne measurements of the optical stratification of aerosols in turbid atmospheres. *Appl. Opt.*, **25,** 4374–4381.

——, ——, M. Yamano, M. Shiobara, K. Arao, and Y. Nakanishi, 1989: Aerosol optical characteristics in the yellow sand events observed in May, 1982 in Nagasaki—Part II Model. *J. Meteor. Soc. Japan,* **67,** 279–291.

Pilewskie, P., and F. P. J. Valero, 1992: Radiative effects of the smoke clouds from the Kuwait oil fires. *J. Geophys. Res.*, **97,** 14 541–14 544.

Rao, C. R. N., L. L. Stowe, E. P. McClain, and J. Sapper, 1988: Development and application of aerosol remote sensing with AVHRR data from the NOAA satellites. *Aerosols and Climate,* P. V. Hobbs and M. P. McCormick, Eds., A. Deepak Publishing, 69–79.

Shiobara, M., and S. Asano, 1994: Estimation of cirrus optical thickness from sun photometer measurements. *J. Appl. Meteor.*, **33,** 672–681.

Stowe, L. L., R. M. Carey, and P. P. Pellegrino, 1992: Monitoring the Mt. Pinatubo aerosol layer with NOAA/11 AVHRR data. *Geophys. Res. Lett.*, **19,** 159–162.

Tanre, D., C. Devaux, M. Herman, and R. Santer, 1988: Radiative properties of desert aerosols by optical ground-based measurements at solar wavelengths. *J. Geophys. Res.*, **93,** 14 223–14 231.

Weiss, R. E., and P. V. Hobbs, 1992: Optical extinction properties of smoke from the Kuwait oil fires. *J. Geophys. Res.*, **97,** 14 537–14 540.

——, V. N. Kapustin, and P. V. Hobbs, 1992: Chain-aggregate aerosols in smoke from the Kuwait oil fires. *J. Geophys. Res.*, **97,** 14 527–14 531.

Young, A. T., 1981: On the Rayleigh-scattering optical depth of the atmosphere. *J. Appl. Meteor.*, **20,** 328–330.